2016

Study of x-rays produced from debris-free sources with Ar, Kr and Kr/ Ar mixture linear gas jets irradiated by UNR Leopard laser beam with fs and ns pulse duration

V. L. Kantsyrev
University of Nevada, vlkantsyrev@gmail.com

K. A. Schultz
University of Nevada

V. V. Shlyaptseva
University of Nevada

A. S. Safronova
University of Nevada

I. K. Shrestha
University of Nevada

See next page for additional authors

High Energy Density Physics 19 (2016) 11–22

Contents lists available at ScienceDirect

High Energy Density Physics

journal homepage: www.elsevier.com/locate/hedp

Study of x-rays produced from debris-free sources with Ar, Kr and Kr/Ar mixture linear gas jets irradiated by UNR Leopard laser beam with fs and ns pulse duration

V.L. Kantsyrev [a,*], K.A. Schultz [a], V.V. Shlyaptseva [a], A.S. Safronova [a], I.K. Shrestha [a], G.M. Petrov [b], J.J. Moschella [a], E.E. Petkov [a], A. Stafford [a], M.C. Cooper [a], M.E. Weller [a,1], W. Cline [a], P. Wiewior [a], O. Chalyy [a]

[a] Physics Department, University of Nevada, Reno, Nevada 89557, USA
[b] Plasma Physics Division, Naval Research Laboratory, Washington, DC 20375, USA

ARTICLE INFO

Article history:
Received 21 October 2015
Received in revised form 11 February 2016
Accepted 13 February 2016
Available online 23 February 2016

Keywords:
Laser plasmas
Gas jet
Clusters
X-ray emission

ABSTRACT

Experiments of x-ray emission from Ar, Kr, and Ar/Kr gas jet mixture were performed at the UNR Leopard Laser Facility operated with 350 fs pulses at laser intensity of 2×10^{19} W/cm^2 and 0.8 ns pulses at an intensity of 10^{16} W/cm^2. Debris free x-ray source with supersonic linear nozzle generated clusters/monomer jet with an average density of $\geq 10^{19}$ cm^{-3} was compared to cylindrical tube subsonic nozzle, which produced only monomer jet with average density 1.5–2 times higher. The linear (elongated) cluster/gas jet provides the capability to study x-ray yield anisotropy and laser beam self-focusing with plasma channel formation that are interconnecting with efficient x-ray generation. Diagnostics include x-ray diodes, pinhole cameras and spectrometers. It was observed that the emission in the 1–9 keV spectral region was strongly anisotropic depending on the directions of laser beam polarization for sub-ps laser pulse and supersonic linear jet. The energy yield in the 1–3 keV region produced by a linear nozzle was an order of magnitude higher than from a tube nozzle. Non-LTE models and 3D molecular dynamic simulations of Ar and Kr clusters irradiated by sub-ps laser pulses have been implemented to analyze obtained data. A potential evidence of electron beam generation in jets' plasma was discussed. Note that the described debris-free gas-puff x-ray source can generate x-ray pulses in a high repetition regime. This is a great advantage compared to solid laser targets.

1. Introduction

The development of efficient debris-free x-ray probes with photon energies 1–20 keV (~0.6–12 Å) is important for high-energy density physics (HEDP) research at large scale facilities such as NIF and OMEGA [1]. The goal of our studies is a better understanding of the mechanisms of laser-to-x-ray energy conversion (both thermal and non-thermal) and the directionality of x-rays. These studies are not only of academic interest, but might also lead to very important applications of novel x-ray sources for low-energy (<15–20 keV) x-ray effects testing and x-ray backlighting researches. For purity of experiments, x-ray sources for such researches should have maximum x-ray yield and at the same time generate minimum ion and electron beams, and neutral solid micro-particles and liquid droplets debris. Protection from ion and electron beams can be provided by application of strong magnets that will deflect beams. But neutral components can be stopped only with filters that will absorb a lot of x-rays (especially in medium and soft spectral regions). Even modern solid targets consisting of flat surfaces coated with nanotubes generate a lot of debris in the form of solid micro-particles and liquid droplets during emission of x-rays [2]. In the same time, cluster/gas medium as a fs laser target exhibiting the advantages of both solid and gaseous targets does not generate solid micro-particles and liquid droplets [3].

Clusters are produced as a result of spontaneous condensation in a super-cooled gas outflow from a nozzle. The target is considered as a two-phase medium, which consists of continuous gas phase and discrete condensed phase clusters [4]. Typically, in high-pressure (a few atmospheres) gas jets with densities of around 10^{19} cm^{-3}, clusters with diameters of several tens of Å, and 10^3–10^4 particles per cluster, are formed. The cluster lifetime τ_c is limited by hydrodynamic expansion or Coulomb explosion to 10–100 fs.

* Corresponding author. Physics Department, University of Nevada, Reno, Nevada 89557, USA.
E-mail address: vlkantsyrev@gmail.com (V.L. Kantsyrev).
[1] Current address: Lawrence Livermore National Laboratory.

http://dx.doi.org/10.1016/j.hedp.2016.02.001
1574-1818/

Plasma is formed when the target (cluster or gas) is ionized by laser radiation via optical field ionization and/or collisional ionization [5]. The latter is negligible for gas jets, but important for clusters due to the high background plasma density within the cluster. Clusters and gas jets share common features, but clusters are better suited than gas jets due to their unique properties and dynamics. Both form low-density plasma, but clusters start at solid density, which after irradiation is converted into high-density plasma (n_e ~10^{23}–10^{24} cm^{-3}) capable of absorbing the laser radiation with high efficiency. Cluster explosion converts it back into low-density plasma, but the short-lived intermediate state (as a cluster) is crucial.

In this paper, we focus on investigation of pulsed debris-free radiation source where x-rays are produced as a result of the interaction of a laser pulse with cluster/gas jet. Supersonic cluster/gas jet configuration, namely linear, was applied during experiments. The influence of the composition of gas (Ar, Kr, or Kr/Ar mixture) on x-ray yield was studied. Also, a comparison of the x-ray yield from the same jet but with different pulse duration (350 fs – short pulse or 0.8 ns – long pulse) was performed. A pulse contrast ratio was of 10^{-7}. In experiments with Ar, the x-ray yield and spectra from supersonic linear jet were compared with subsonic cylindrical jet. Linear (elongated) jets provide the possibility of the study of x-ray yield anisotropy. Also, experiments with non-linear processes of laser beam self-focusing [6] when laser beam propagates along the linear nozzle are possible. The harder x-ray emission is interconnecting with self-focusing processes [7]. Most of the early experiments on the investigation of ultra-short laser pulse interaction with cluster/gas jet were performed with conical nozzles [8–12], but linear jets were not studied sufficiently yet [13–15].

At the same time, we try to improve cluster ionization efficiency and x-ray yield by adding easily ionizable seed heavy atoms (for example, Kr with ionization potential of outer electron $I_p = 14$ eV) to the lighter carrier gas (Ar with $I_p = 16$ eV). Indeed, clusters formed from Kr (in Kr/Ar mixture jet) might have higher electron density (n_e) produced by the initial laser ionization than pure Ar clusters, that will enhance the x-ray yield, and higher charge states that will shift the x-ray radiation toward higher energies (shorter wavelengths). Internal degrees of freedom of the heavier seed gas are cooled by the carrier gas (Ar); therefore, the seed gas (Kr) will be clustering more efficiently, and it will be accelerated to Ar velocity V_{cAr} (even more, carrier gas Ar might be not clustered at all [16]). All of the above may contribute to increase the x-ray yield, as well as extend the x-ray spectra range, compared to pure Ar or Kr jets.

Experimental details of the experiments are given in Section 2. Results of experimental studies of x-ray emission from Ar, Kr, and 15%Kr/85%Ar mixture (the percentage concentration of gases in the mixture are in partial pressure) jets are presented and discussed in Section 3. The concluding remarks are in Section 4.

2. Experimental details

The experiments were performed at the UNR Leopard laser. This system is a hybrid 1.057 μm Ti : Sapphire/Nd : glass laser system that generates up to 10–15 J in short pulses ($\tau_{las} = 350$ fs) or 20–25 J in long pulses ($\tau_{las} = 0.8$ ns). Later in the text we will use the terms "short laser pulse" and "long laser pulse". The laser pulse pedestal was about 15 mJ with duration 3 ns (in laser short pulse regime). The main ultra-short pulse was positioned in the middle of pedestal. The laser pulse contrast (ratio between the laser peak intensity I_{peak} and pedestal pulse intensity I_p) in this case was around 10^{-7}. The laser beam was focused by f/1.5 off-axis parabola mirror in the center of the linear cluster/gas jet (Fig. 1) along longitudinal jet cross-section axis and perpendicular to jet propagation direction, or in the center of cylindrical jet perpendicular to jet propagation direction. The focal spot size was 10 μm, producing pulses with an intensity of around

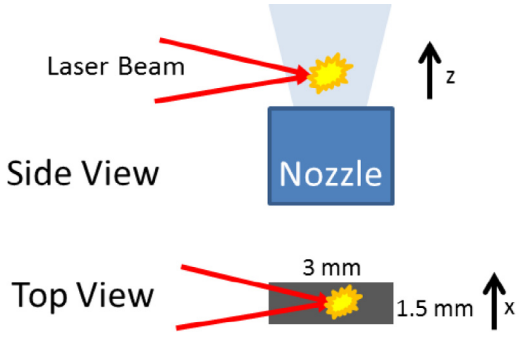

Fig. 1. Scheme of the experiment with supersonic nozzle (view from the side is at the top, view along central jet axis is at the bottom). Laser beam focused by parabolic off-axis laser mirror is shown in solid lines, cluster/gas jet is light gray, and the laser-produced plasma is shown as a star. Laser beam polarization is directed along Z axis. The distance between nozzle and the focal spot was varied from 1 to 3 mm during experiments.

2×10^{19} W/cm^2 in the short pulse regime and 10^{16} W/cm^2 in the long pulse regime. The focusing point was placed at a distance of 1–3 mm from the nozzle's exit. The jet propagation direction was parallel to the laser beam polarization axis. Linear jets were generated by a linear nozzle (output cross-section was 1.5×3 mm) mounted to the Parker Co. Series 9 pulsed gas valve with a 350 μs opening time (backing pressure was varied from 500 psi to 700 psi). The linear nozzle profile provides supersonic speeds at the output cross-section (for example, for Ar the Mach number was about M = 4). Later it will be named "supersonic nozzle" throughout the text. In some experiments a simple subsonic tube nozzle (inner diameter $\phi = 2.4$ mm) has been used for comparison with the supersonic nozzle results. Later it will be named "subsonic nozzle" throughout the text.

The nozzles were placed on a translational mount (remotely moving in three orthogonal directions) in the center of the Phoenix vacuum chamber with an operational vacuum of 5×10^{-5} torr.

The diagnostics consist of time-resolved and time-integrated devices (Fig. 2). Time-resolved x-ray diagnostics include: three sets of filtered x-ray detectors (absolutely calibrated PCD [diamond photoconductive detectors] with filter cut-off energy 2.4 keV, and three cross-calibrated AXUV-HS5 Si-diodes with filter cut-off energies 1.4, 3.5 and 9 keV) and two Faraday cup detectors with 4 μm Al filters (electron cut-off energy 19 keV). The timing of all these detectors signals was measured in correlation with the gas delay time. The

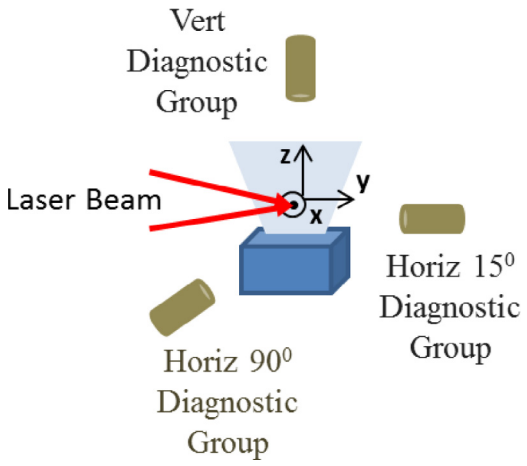

Fig. 2. Scheme of x-ray and electron beams diagnostics positions in experiment with linear nozzle.

gas delay time was defined as the interval between energizing of the pulsed valve and the moment the laser pulse interacts with the gas jet. Time-integrated x-ray diagnostics include two three-channel pinhole cameras (cut-off energies 0.7, 1.4 and 3.5 keV) with a spatial resolution of 60 μm. Also, we applied three x-ray spectrometers: a Johann type with Si crystal (spectral resolution $\lambda/\Delta\lambda = 1200$), a Hamos type with mica crystal ($\lambda/\Delta\lambda = 500$), and a convex crystal spectrometer with KAP (potassium biphthalate) crystal ($\lambda/\Delta\lambda = 500–700$). Of the three diagnostic groups, the two horizontal sets were placed near perpendicular to the laser beam polarization, one aligned near 15° to the laser beam propagation direction and the second set near 90° to the laser beam propagation. The vertical group was placed parallel to the laser beam polarization and perpendicular to beam propagation direction. The pinhole cameras and Faraday cups were typically in the 15° horizontal and vertical groups. X-ray spectrometers were positioned near the horizontal group at 90° to the laser beam polarization and its propagation.

Note, that during preliminary experiments, it was found that the maximum x-ray yield corresponds to a laser beam focus at 1 mm from the exit of the supersonic nozzle [17].

We have used our optical diagnostics to characterize the cluster/monomer jets and make a preliminarily determination of cluster size and average density of the gas jets with high resolution interferometry [18] and Rayleigh scattering systems [19]. The resulting data are used to optimize x-ray yields from jets when interacting with short pulse laser beams. Interferometry is a common laser-based diagnostic that can be used to measure the gas jet density. The interferometric measurement yields the phase shift of the laser light integrated along the path of the laser beam through the gas jet. The phase shift is directly related to the index of refraction, *n*, which, in turn, is related to the gas jet density. The 2D interferograms were created using a standard Mach–Zehnder interferometer where a pulsed laser beam (532 nm) was collimated into a 1-inch diameter beam. Beam-splitters (2-inch diameter) were used to form and recombine the scene and reference arms, and a lens was used to project the image onto a CCD camera having a 1317×1095 pixel array. The interferometer's laser pulse was short enough (~6 ns) so that the gas distribution can safely be assumed as constant over the duration of the pulse. An interferometric analysis software program was used to calculate the line integrated density of our supersonic jets. It applied the well-known Fourier transform technique [18] from which line-integrated density information is obtained for all pixels within a rectangular region of the interference pattern. Using this technique, the maximum average jet densities at 1 mm from nozzle (position of short pulse laser beam focusing point) were calculated based on line integrated density measurements. For Ar and Kr gas jets we measured $N_{Ar} = 2.77 \times 10^{19}$ cm^{-3}, $N_{Kr} = 1.67 \times 10^{19}$ cm^{-3}, respectively. The Rayleigh scattering system was applied to measure the so called main cluster parameter ηN_c that can be used to recover the average cluster radius R_c within the jet ($R_c = N_c^{1/3} \times R_{at}$, where R_{at} is the weighted average radius of atom). Here, η is the fraction of atoms in the cluster state and N_c is the average number of atoms in the cluster. For the scattering apparatus [19], we used a continuous 2 W, 445 nm diode laser in conjunction with a gated intensified CCD (ICCD) camera. A single lens was used to focus the laser at the gas jet to improve spatial resolution. For Ar, ηN_C is very strongly dependent on the distance from a nozzle exit, in contrast to Kr and the 15%Kr/85%Ar mixture. For Ar and Kr, we determined: $R_c = 16$ Å and $R_c = 14$ Å, respectively, at a distance of approximately 1 mm from the nozzle, assuming that $\eta = 1$. The mixture of 15%Kr/85%Ar has a profile more like pure Kr than pure Ar, and larger ηN_c than Kr at distance of 1 mm from the nozzle (typical position of short pulse laser beam focusing point). In experiments with the subsonic tube nozzle no clusters were observed and jet average density was of 1.5–2 times higher in comparison with linear nozzle.

3. Experimental studies of x-ray emission from Ar, Kr, and 15%Kr/85%Ar mixture jets

Experiments show that laser irradiated cluster/monomer jets work as debris-free sources of x-ray radiation. We found that thin test-objects (such as several μm thick Al, Ti, or Cu foils) placed near the laser focusing point in jets (2–4 cm distance) at 90° to laser beam axis exhibit only thermal and ion beam damages from the nearby plasma. No holes in tested foils were found in contrast with experiments using thin flat laser targets. In this case many holes in tested foils appeared after the first laser shot [20].

X-ray bursts produced from pure Ar, pure Kr, or a mixture of 15%Kr/85%Ar jets irradiated by short laser pulses [350 fs] at an intensity of 2×10^{19} W/cm^2, were found to last from 2 to 7 ns (Figs. 3, 4). In all spectral regions, the shapes of the x-ray bursts were similar: a sharp forefront, and a gently sloping trailing edge (Figs. 3, 4). We are not able to estimate real duration of x-ray burst forefront due to low time resolution of our x-ray detectors (0.5–0.7 ns) at this time.

3.1. Experimental study of x-ray emission from sources with Ar and Kr jets

In this section, we report the x-ray emission from Ar linear jets due to interaction with long and short laser pulses. It was observed that for a laser pulse with an energy of 15 J and comparable jet parameters (500–600 psi, gas delay time around 700–1000 μs) the short laser pulse generates a higher x-ray burst in the 3.5 keV range than the long pulse (Fig. 4). In all experiments the gas delay is measured from the time the valve energizing to gas jet interaction with the laser.

We also compared x-ray emission from supersonic and subsonic nozzles. Comparison of x-ray emission from Ar gas jets produced by supersonic and subsonic nozzles and irradiated by the short fs laser pulses show that supersonic jets (with clusters) radiated much more energy in both 1.4 keV and 3.5 keV spectral regions (Fig. 5). The observed effect of changing gas delay time (i.e., the initial density of jet) on x-ray yield offers some control over property of emitted radiation. It is an advantage of using the jet targets unique to gas-puffs.

The x-ray images of Ar plasma from supersonic and subsonic nozzles appear to be different (Fig. 6).

X-ray spectroscopic studies of laser pulse interaction with Ar jets were performed to better understand the plasma conditions. Initially, x-ray spectra were recorded from the interaction of a long pulse with the supersonic jet and subsonic jet (Fig. 7).

The spectroscopic data of the long pulse interaction with the subsonic jet without clusters (Fig. 7) were very different from the supersonic jet (not shown here because of a poor quality of the spectrum). In particular, for the long pulse and supersonic jet, the spectral features from the highest ionization stages such as He-like and Li-like Ar to Be-like Ar to the lower ionization stages such as B- to F-like Ar as well as a very broad "cold" Kα line (which likely to include lines from neutral to Ne-like Ar ions) were observed. The presence of a whole sequence of ionization stages together with the "cold" Kα line is likely to indicate the existence of the electron beams with non-Maxwellian distribution in plasma of a moderate electron temperature Te (somewhat between 200 eV and 500 eV, which we were not able to estimate more accurately because of a poor quality of the spectrum for this particular laser experiment). Note that during experiments with Ar, signals from Faraday cup detectors of electrons were observed sporadically. In addition, such x-ray spectra are very similar to K-shell Ar spectra from plasma focus from Reference 21 discussed in Reference 22 where it was stated that the main features of the plasma focus were a relatively low plasma temperature and the presence of an electron beam. Interestingly, these

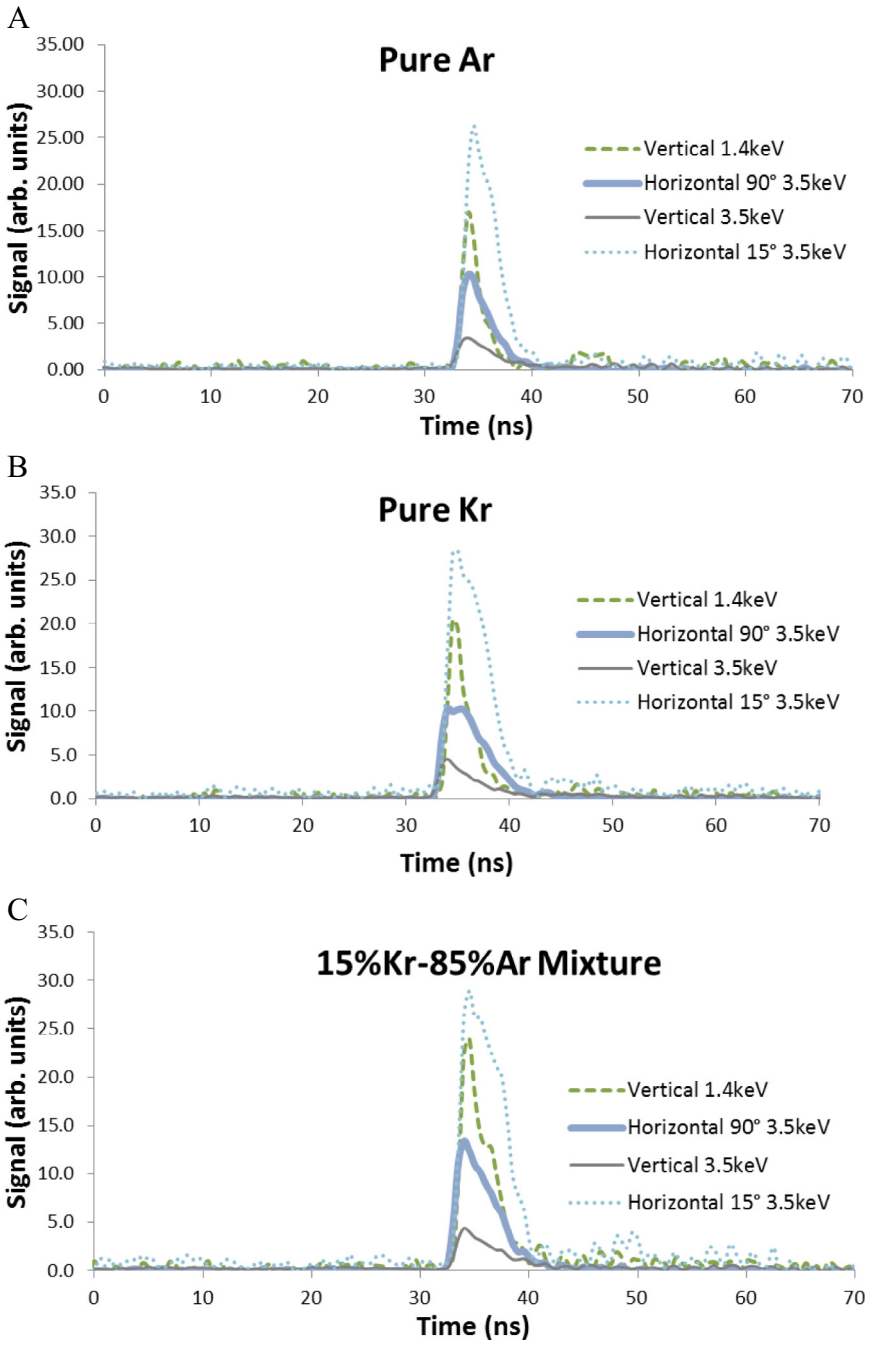

Fig. 3. Non-normalized x-ray bursts from pure Ar (A, shot #1295), Kr (B, shot # 1300), and 15%Kr–85% Ar mixture (C, shot # 1304) jets (delay time 1000 μs, backing pressure 600 psi) at intensity 2×10^{19} W/cm^2. The distance between laser beam axis and nozzle output was 1 mm.

K-shell Ar spectra (produced with a long pulse) are somewhat different from the ns-laser plasma spectra shown in [22] that displayed only He-like and Li-like Ar spectra and no lower ionization stages and "cold" Kα line.

However, for the long pulse but subsonic jet, only "cold" Kα line was recorded that also manifests in the 2nd and the 3rd order lines (Fig. 7). Multiple lines in the 2nd and the 3rd order indicate several x-ray sources in the plasma. Lack of Ar He_α and additional satellite lines suggests that a much cooler and uniform plasma with temperature in the range Te = 10–30 eV was formed. Observation of "cold" Kα can be explained by the existence of a strong electron beam in the laser generated plasma without clusters. It is important to emphasize that the similar spectrum to the one in Fig. 7 (with just an Ar "cold" Kα line) was obtained when the short laser pulse interacted with the subsonic jet without clusters.

The spectroscopic results of the interaction of the short laser pulse with the Ar supersonic jet help to explain the higher radiation yield from supersonic jets (Fig. 8). Two non-local thermodynamic equilibrium (non-LTE) Ar and Kr models were developed in order to model experimental spectra produced from experiments with a supersonic cluster/gas jet in this paper. Both of these models include ground states form bare to neutral atoms. In particular, the Ar model is detailed from H- to Ne-like while the Kr model is detailed from H- to Al-like. Singly excited states are included for both models up to n = 6 for H-like ions, n = 5 for He- to Li-like ions and Ne-like–Na-like ions, and n = 4 for Be- to F-like ions and Mg- and Al-like ions.

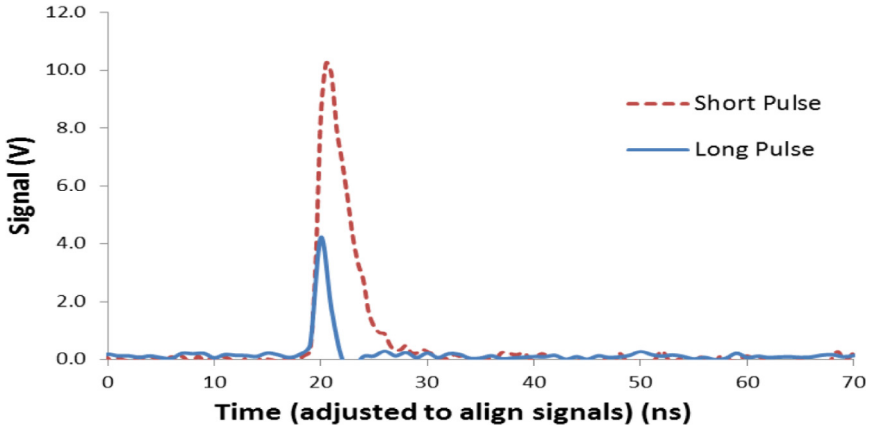

Fig. 4. Example of x-ray burst measured by Si diodes (in region >3.5 keV) from linear Ar jets irradiated by the Leopard laser using short and long pulses. The distance between laser beam axis and nozzle output was 1 mm.

The atomic data for both models was calculated using the Flexible Atomic Code [23]. Voigt line profiles are used to construct the spectra in order to take into account the effects of Doppler broadening and natural broadenings in the plasma, as well as instrumental broadening due to limited resolution of the detector. Synthetic spectra can be generated from each model dependent on plasma parameters such as electron temperature, electron density (n_e), and parameters of the non-Maxwellian distribution function to include hot electrons (see, for example, [24]).

Using the non-LTE Ar model, the theoretical fit of the x-ray spectrum in Fig. 8 gives Te ~750 eV and n_e ~5×10^{20} cm^{-3}, but underestimated Be-like satellite structure, which was modeled separately at different conditions. Also, there is no evidence of "cold" Kα, which correlated with very low or even absence of signals from Faraday cup detectors. Interestingly, K-shell Ar spectrum from the short laser pulse in this paper resembles again the spatially resolved K-shell Ar spectrum from plasma focus [21], but recorded at approximately 2 cm from the anode (similar distribution of intensities between the most intense Heα line, He IC line, Li-like peak, and weak Be-like peak and almost no lower ionization stages as well as a very weak "cold" Kα) and not the fs-laser pulse K-shell Ar spectra presented in References 22 and 25, which display more intense lower ionization stages and are generated by much lower pulse duration (30–60 fs). In particular, the Boltzmann equation and a detailed collisional-radiative model were solved simultaneously as a function of time to model the time-integrated x-ray spectra of the transient plasma produced by a high intensity ultrafast laser source in Reference 25. It was shown that the typical Li-like and Be-like Ar satellite structure, sometimes attributed to a hot-electron component in the electron distribution function, can also be due to transient effects in a high temperature ionizing plasma [25]. Because our K-shell Ar spectra do not express spectral features that were modeled and discussed in Reference 25 and also our short pulse experiments had much longer pulse (350 fs vs 30–60 fs), we do not see manifestation of the transient plasma effects, but may have some of hot electron effects.

We have performed experiments with the supersonic nozzle using Kr gas and compared results with Ar gas data. An important parameter that characterizes the x-ray gas-puff source with the supersonic nozzle is the coefficient of conversion ε of laser pulse energy to x-ray output in one of the specific spectral ranges used in x-ray backlighting studies (for example near 2–3 keV). The conversion coefficient was determined through the use of two absolutely calibrated PCDs for supersonic Kr and Ar jets from the nozzle operated with optimum backing pressure and gas delay time to obtain maximum x-ray output (Fig. 9). The PCDs were placed in different positions relative to nozzle exit. The "horizontal" 2.4 keV filtered PCD was placed perpendicular to the laser beam polarization direction and aligned near 15° to laser beam propagation direction. The "vertical" 2.4 keV filtered PCD was placed near 30° to the laser beam polarization direction and near 60° to laser beam propagation direction. Measurements were performed at various distances

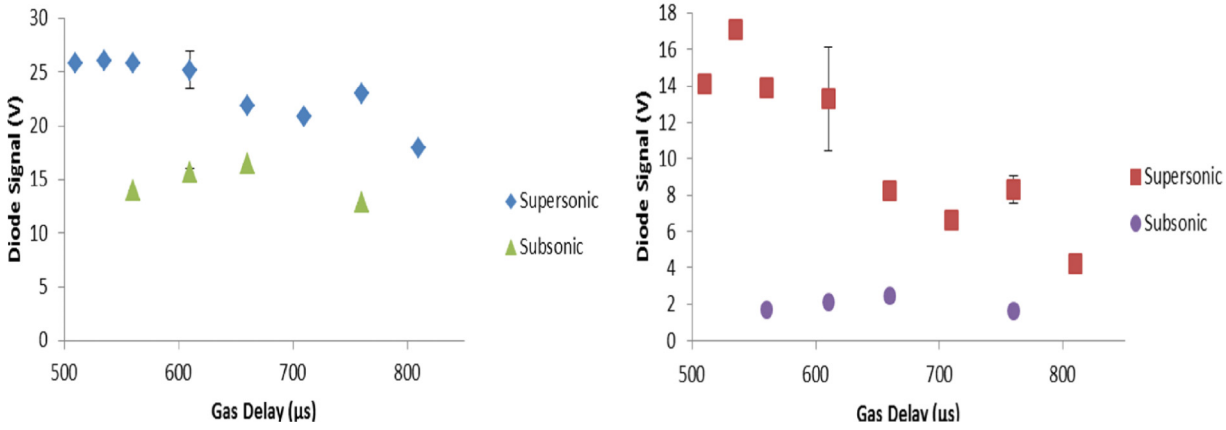

Fig. 5. Comparison of X-ray emission detected by filtered Si-diodes from Ar gas jets produced by supersonic and subsonic nozzles. The Ar gas jets with a backing pressure of 500 psi. Left: results for >1.4 keV region, right: data for >3.5 keV region. Short laser pulse.

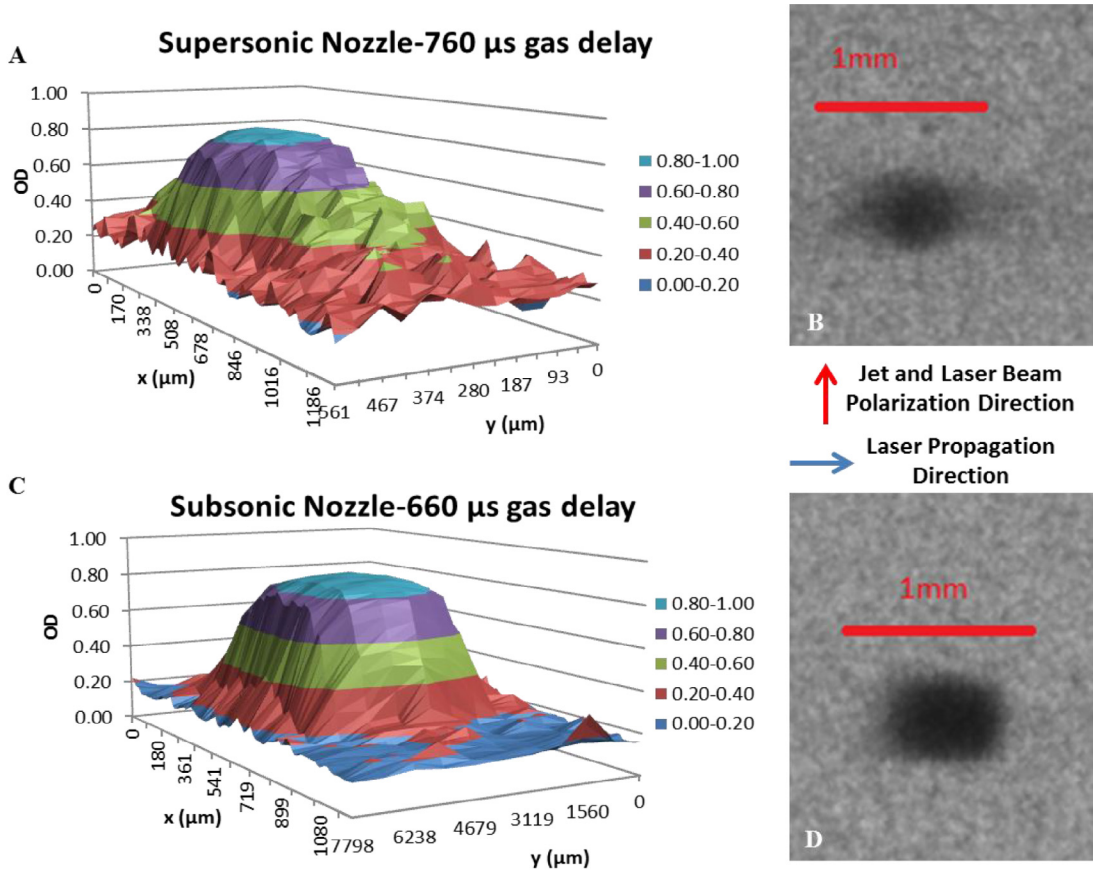

Fig. 6. Time integrated x-ray pinhole images of Ar laser plasma from supersonic (A and B) and subsonic (C and D) nozzles. OD is optical density of x-ray images on film Kodak Biomax MS. Laser beam propagated along x-axis. The scale added to pinhole images is 1 mm. Spatial resolution is 60 μm and filter cut-off energy is 1.4 keV. Distance between laser beam axis and nozzle output was 1 mm. Backing pressure was 500 psi.

between the laser focus point and linear nozzle exit. The first important new observation was an anisotropy of the 2.4 keV x-ray output: the maximum x-ray radiation was mainly emitted along the laser beam propagation and perpendicular to laser beam polarization direction ("horizontally"). This behavior was characteristic for both Kr and Ar supersonic jets. The maximum value of ε in the spectral region >2.4 keV exceeded 5×10^{-4}. For comparison, our previous measurements yielded a conversion efficiency of $\varepsilon = 2.5 \times 10^{-3}$ in the spectral region >0.7 keV, which can also be used for x-ray backlighting. We explained the observed anisotropy of x-ray radiation later in the text. The second important new finding was that the absolute x-ray output from of supersonic jets of Kr and Ar plasma depended on the laser focus distance from nozzle. The conversion coefficient was measured when moving away from the nozzle exit. The maximum ε was observed at laser beam focus point 1 mm from the nozzle exit.

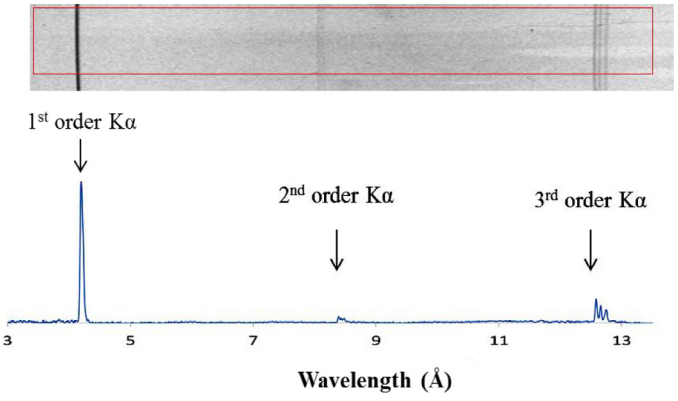

Fig. 7. Ar x-ray spectra produced using subsonic gas jet (long laser pulse). A convex crystal spectrometer with KAP crystal. Laser energy – 18 J. Laser flux density ~3×10^{16} W/cm^2 in 10 μm size focusing spot. Distance between laser beam axis and nozzle output was 1 mm.

Observation of 2–4 transitions with high spectral resolution of $\lambda/\Delta\lambda$ ~1200 (a Johann type spectrometer) provides an excellent test bed for modeling of x-ray spectra of Kr (Fig. 10). The spectroscopic modeling of radiation emitted during the interaction of short laser pulse with the Kr supersonic jet indicate the dominance of the Na-like and Ne-like Kr spectral features and thus lower temperature and higher plasma density compared to Ar: Te = 400 eV and n_e ~10^{21} cm^{-3}. However, the non-LTE modeling of such spectra at lower Te but with a small fraction of hot electron (1–3%) may lead to a very similar fit, what was discussed in detail in Reference 26 and therefore it is possible that a few percent of the hot electrons were present in Kr short pulse laser experiments. We also conclude that Kr linear jet can also be an effective x-ray radiator.

Comparison of Kr and Ar supersonic jets x-ray images show that the Kr and Ar plasmas are close in size (Fig. 11). The plasma size was reduced from 1 mm at image cut-off energy 0.7 keV to 0.2 mm when the cut-off energy rises to 3.5 keV. From these observations we concluded that supersonic jets plasmas are highly non-uniform with a compact bright, hot core.

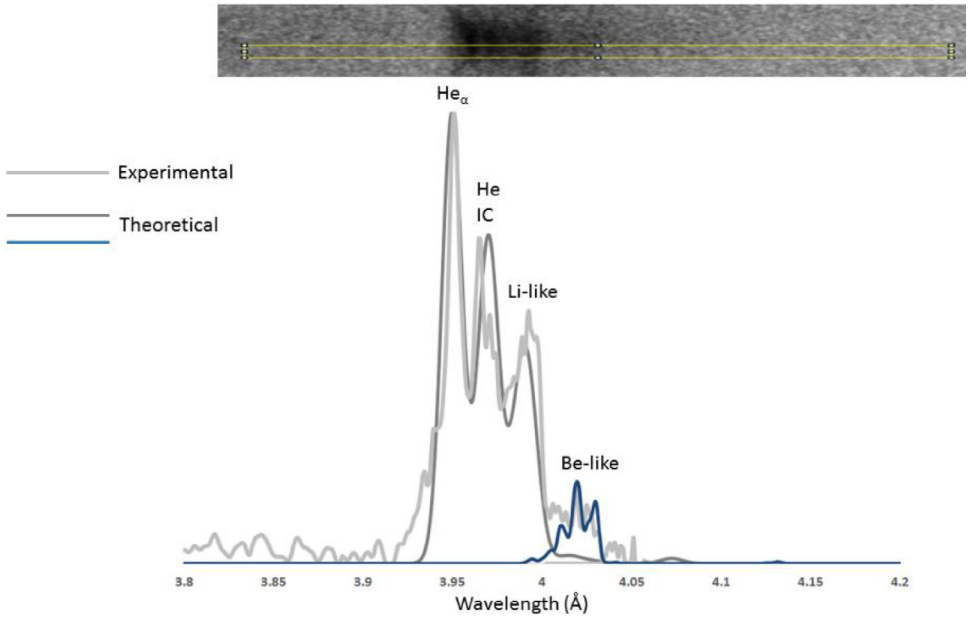

Fig. 8. Ar x-ray spectra results produced in experiments with supersonic cluster/gas jet (short laser pulse). A Hamos spectrometer with mica crystal. Laser energy – 14 J. Laser flux density $\sim 2 \times 10^{19}$ W/cm^2 in 10 μm size focusing spot. Distance between laser beam axis and nozzle output was 1 mm.

3.2. *Theoretical modeling of interaction of short laser pulses with Ar and Kr supersonic jets*

Interaction of short laser pulses with Ar and Kr clusters was modeled using a 3D relativistic molecular dynamics (MD) code [27,28]. The model accounts for plasma formation within the cluster, coupling of laser energy to the plasma and plasma evolution. The latter involves ionization of the atoms/ions due to optical field and collisional ionization with electrons, cluster expansion, electron and ion densities. More importantly, at any given time. the model calculates the cluster radius and ion charge distribution f(q), from which the ion densities $n_i(q,t)$ of any charge state q can be computed. In general, the MD model is coupled to a non-LTE CR model and its output, the electron density $n_e(t)$, temperature $T_e(t)$, and ion densities $n_i(q,t)$, can be used as input for the non-LTE CR model. The latter can determine the population of excited states for each ionization stage, from which the x-ray yield emitted from these states can be calculated. Finally, synthetic spectra can be built to compare to experimental data.

Numerical simulations were performed for Ar and Kr clusters. Their initial density is that of liquid Ar and Kr, respectively. For both the initial cluster radius was 5 nm, corresponding to 9042 atoms per cluster for Ar and 7364 atoms per cluster for Kr, and the initial charge was set to zero (neutral atoms). Periodic boundary

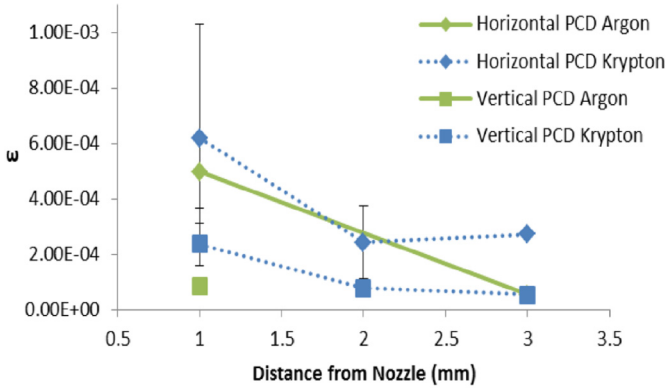

Fig. 9. Conversion coefficient ε of short laser pulse energy to x-rays for Kr and Ar linear jets measured in different directions with respect to laser beam propagation and laser beam polarization, and for varied distance from laser focus point and nozzle exit. Gas backing pressure is 600 psi. Gas delay time is 1000 μs. X-ray detector is filtered PCD with cut-off energy 2.4 keV.

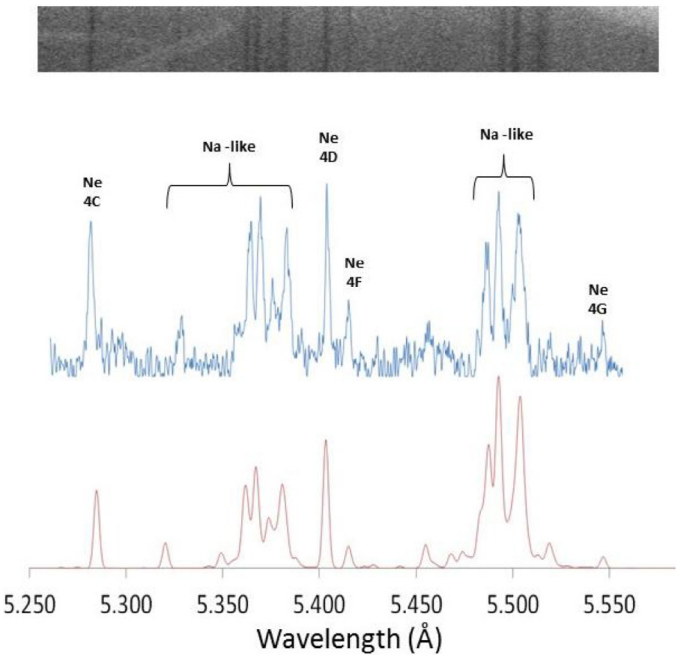

Fig. 10. Kr x-ray spectra results produced in experiments with supersonic cluster/gas jet produced by short laser pulse (top blue line). A Johann type spectrometer with Si crystal. Laser energy was 14.5 J. Laser flux density 2×10^{19} W/cm^2 in 10 μm size focusing spot. Distance between laser beam axis and nozzle output was 1 mm. Theoretical synthetic spectra (bottom red line) calculated at Te = 400 eV and $n_e = 10^{21}$ cm^{-3}.

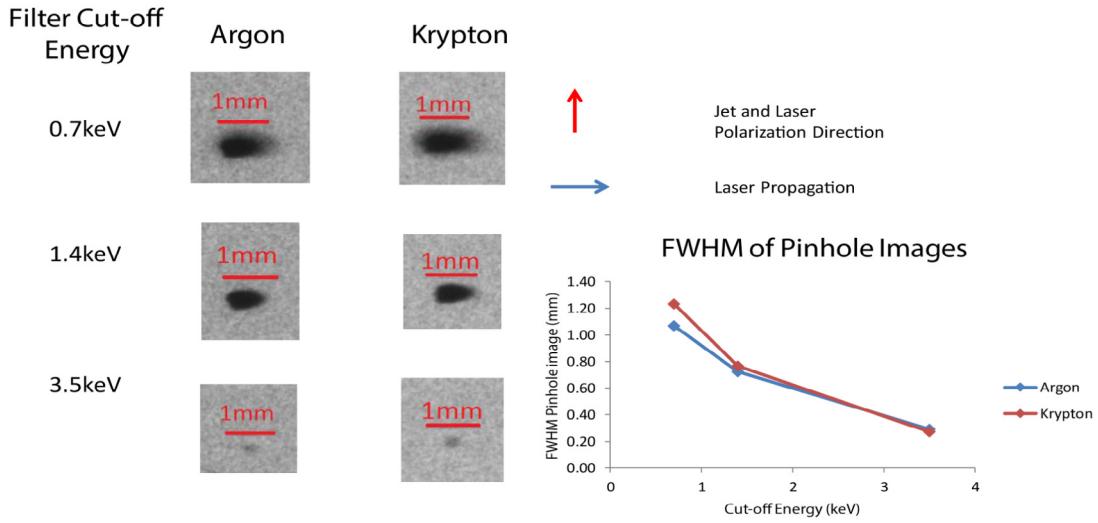

Fig. 11. X-ray pinhole images of x-ray radiation from Kr and Ar linear jets plasma. Short laser pulse (350 fs). Laser flux density 2×10^{19} W/cm^2 in 10 μm size focusing spot. Gas backing pressure is 600 psi. Gas delay time is 1000 μs. Distance between laser beam axis and nozzle output was 1 mm.

conditions were used to account for the presence of adjacent clusters. The inter-cluster distance was 50 nm, about ten times the initial cluster radius.

The numerical simulations show that the interaction of laser radiation with Ar clusters lasts less than 100 fs (Figs. 12, 13). After only 20–30 fs the cluster starts to expand. The cluster expansion accelerates and the electron and ion densities (and clusters density) decrease by 3–4 orders of magnitude. For t > 100 fs the x-ray generation is the result of laser pulse interaction with hot low density Ar plasma as in a gas jet without clusters. There is, however, a profound difference between them. Even though clusters exist only for a very brief period of time and ultimately end as low-density plasma, they can absorb a large fraction of the laser radiation during their short lifetime. This observation can qualitatively explain the shape

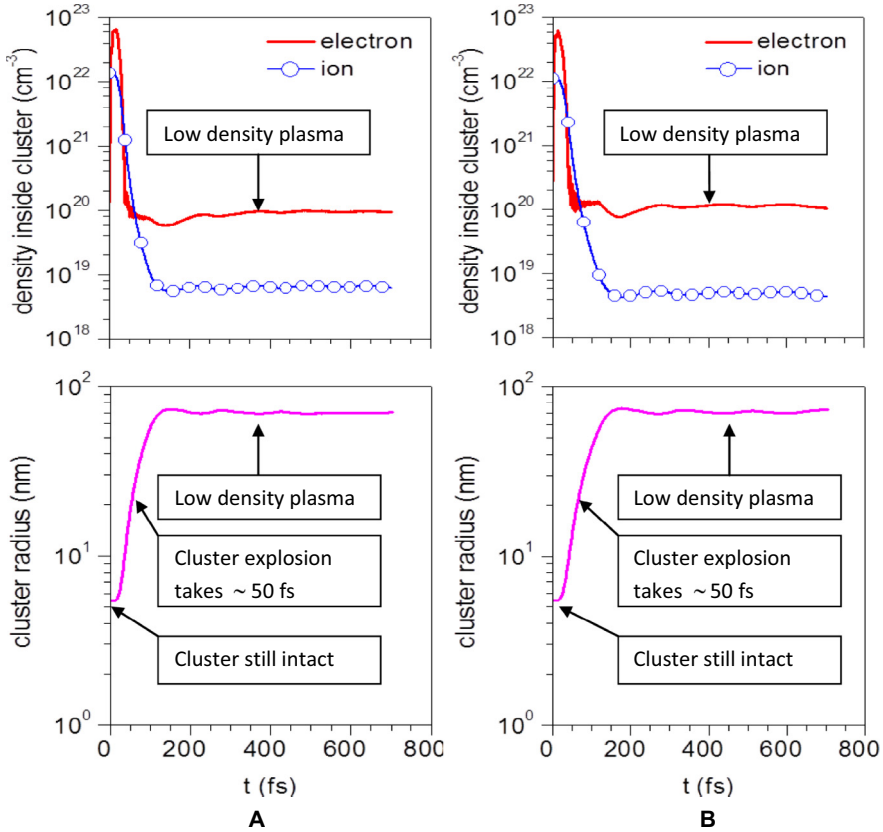

Fig. 12. Simulation results of short laser pulse interacting with Ar clusters. Time evolution of the electron and ion densities inside the cluster (top) and cluster radius (bottom) for Ar (A) and Kr (B). Laser parameters: peak intensity 10^{19} W/cm^2, pulse duration 350 fs (FWHM), wavelength 1 μm. Argon cluster parameters: initial cluster radius 5 nm, number of atoms 9042 and density 1.7×10^{22} cm^{-3}. Krypton cluster parameters: initial radius 5 nm, density 1.4×10^{22} cm^{-3} and number of atoms 7364.

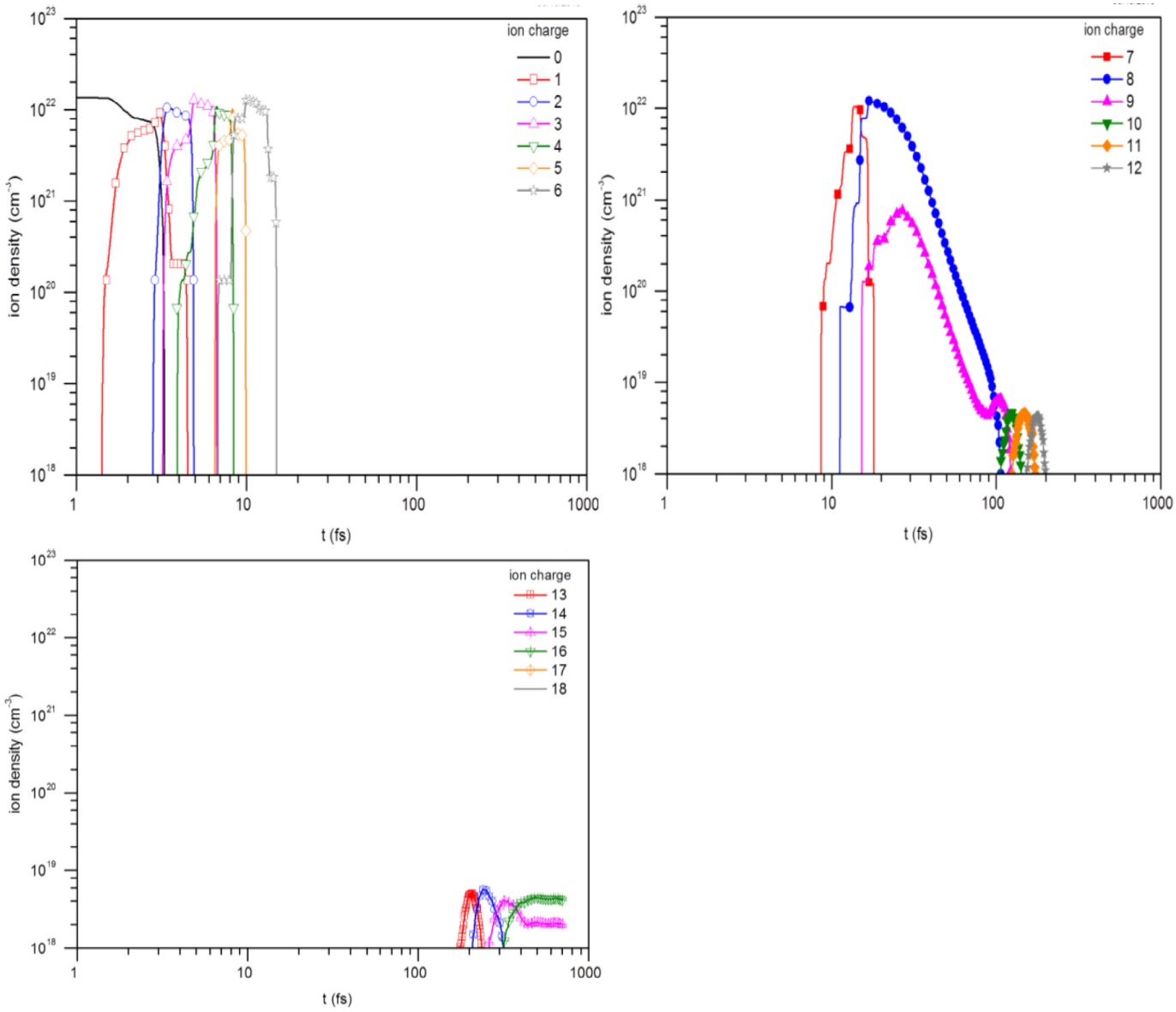

Fig. 13. Time evolution of Ar ion densities with ion charge q from 0 to 6 (top left), 7 to 12 (top right), and 13 to 18 (bottom).

of the observed x-ray pulses, with sharp forefront and gently sloping trailing edge (Figs. 3, 4).

Sequential ionization (optical field and collisional) gradually increases the ion charge and produces highly charged ions, from which soft and hard x-ray emission originates. However, as seen in Figs. 13 and 14, ions with charge $q > 8$ are created only after time $t > 20$ fs, when cluster expansion has taken place and the ion density starts to decrease. As a result, later in time, ions with very high charge are produced (up to Ar^{16+}), but with decreasing density, which asymptotically approaches the density of the gas jet. This is one of the reasons that we observe mostly He-like and Li-like Ar ions in the modeled K-shell Ar spectra (see Fig. 8 and the relevant discussion). Analogous simulations for Kr are shown in Fig. 14: later in time, ions with very high charge are also produced (up to Kr^{25+}), which agrees with the spectroscopic observations. It might be that x-ray bursts with a sharp forefront is due to laser energy resonant absorption by clusters, and then gently sloping trailing edge is due to an interaction of the remaining part of sub-ps laser pulse with low density hot plasma, and after that happened, heating of that low density plasma by trailing end of pedestal pulse (laser post-pulse) and radiative cooling of expanded plasma that contained recombined multicharged ions of Ar or Kr.

3.3. *Experimental study of x-ray emission from source with Ar/Kr mixture jets*

Experiments were performed with two different Ar/Kr mixture supersonic jets: 15%Kr/85%Ar and 5%Kr/95%Ar (the percentage concentration of gases in the mixture is in partial pressure). Laser heating experiments have shown that 15%Kr/85%Ar and 5%Kr/95%Ar have approximately the same x-ray yields in the spectral regions of interest. In the spectral region near 1.4 keV, 5%Kr/95%Ar jet radiated 20% more than 15%Kr/85%Ar, but in the 2.4 keV region the result was opposite. In the region of harder x-ray radiation (>3.5 keV), they radiated at approximately the same level. For this reason, the study was continued with the 15%Kr/85%Ar mixture. K-shell Ar and L-shell Kr x-ray spectra (see the recorded x-ray spectra of L-shell Kr and K-shell Ar and their modeling in Fig. 15), x-ray images, and signals point to different mechanisms of cluster generation in pure Ar and Kr gases compared to mixtures in which Ar plays the role of carrier

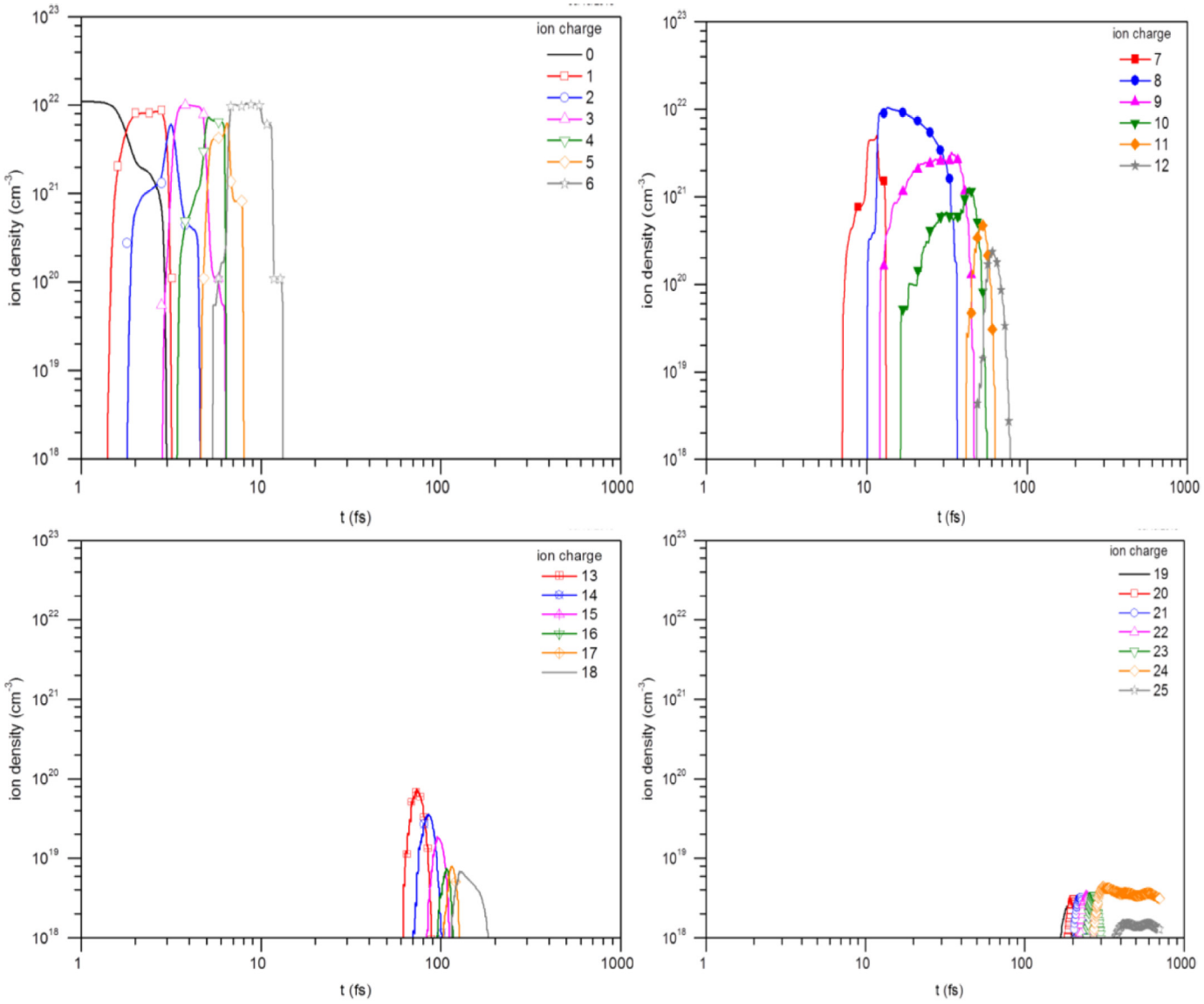

Fig. 14. Time evolution of Kr ions densities with ion charge from 0 to 6 (top left), from 7 to 12 (top right), from 13 to 18 (bottom left), from 19 to 25 (bottom right).

gas and Kr is an additive. The plasma parameters derived for 15%Kr/85%Ar mixture are: for Kr ions $T_e = 450$ eV (somewhat higher than that for pure Kr, Fig. 11), $n_e = 10^{21}$ cm^{-3} (see Fig. 15). However, in Ar plasma, only the K_α line of Ar is observed (Fig. 15), similar to the case when short laser pulses interacted with pure Ar subsonic jet with no clusters (sub-chapter 3.1.). Therefore, we can conclude that in Kr/Ar supersonic jet Ar carrier gas generate clusters inefficiently or even not clustered at all as was predicted in Reference 6.

X-ray bursts from 15%Kr/85%Ar jet lasted from 2 to 7 ns (Fig. 3C). In all spectral regions, the shape of x-ray bursts was similar: sharp forefront with duration smaller than the time resolution of x-ray detectors (0.5 ns), and gently sloping trailing edge (up to 7 ns). Taking into account that Ar might not form clusters in 15%Kr/85%Ar jet irradiated by short laser pulse [17], the x-ray burst from this mixture was similar to that from Kr jet. A comparison of yields from 15%Kr/85%Ar jet vs Ar and Kr jets is shown in Table 1. The measured conversion coefficient of laser energy to x-ray in spectral region >2.4 keV was around $\varepsilon \sim 10^{-4}$–10^{-3}. This result is close to data obtained with conical supersonic nozzles for Ar and Kr jets [10,11].

Data from Table 1 and Fig. 16 demonstrates that x-ray radiation from 15%Kr/85%Ar jet is emitted anisotropically, with maximum emission radiated perpendicular to the laser beam polarization, as for Ar and Kr jets. Experimental deviation of x-ray yield measurements was around ±15%. The degree of anisotropy (ratio of "horizontal" to "vertical" yields) is about 5. The 15%Kr/85%Ar jet radiated more than 20% higher than pure Kr and 50% higher than pure Ar ("horizontal" diagnostic group data) in the spectral range >2.4 keV.

The anisotropy of x-ray emission intensity from 15%Kr/85%Ar jet varied in different spectral regions: it is smaller in the softer x-ray range (>1.4 keV, >2.4 keV) and rising with increasing x-ray photon energy (>3.5 keV and >9 keV). It appears that the temperature of bulk plasma (that connected with the slope of the x-ray integrated intensity distribution to photon energy axis) is also anisotropic (Fig. 16). It is higher near the "horizontal" 15° direction (slope is smaller) and lower near the 90° direction (slope is higher).

4. Conclusion

X-ray emission from a debris-free gas-puff x-ray source using Ar, Kr, and Kr/Ar jets irradiated by long and short laser pulses at a laser

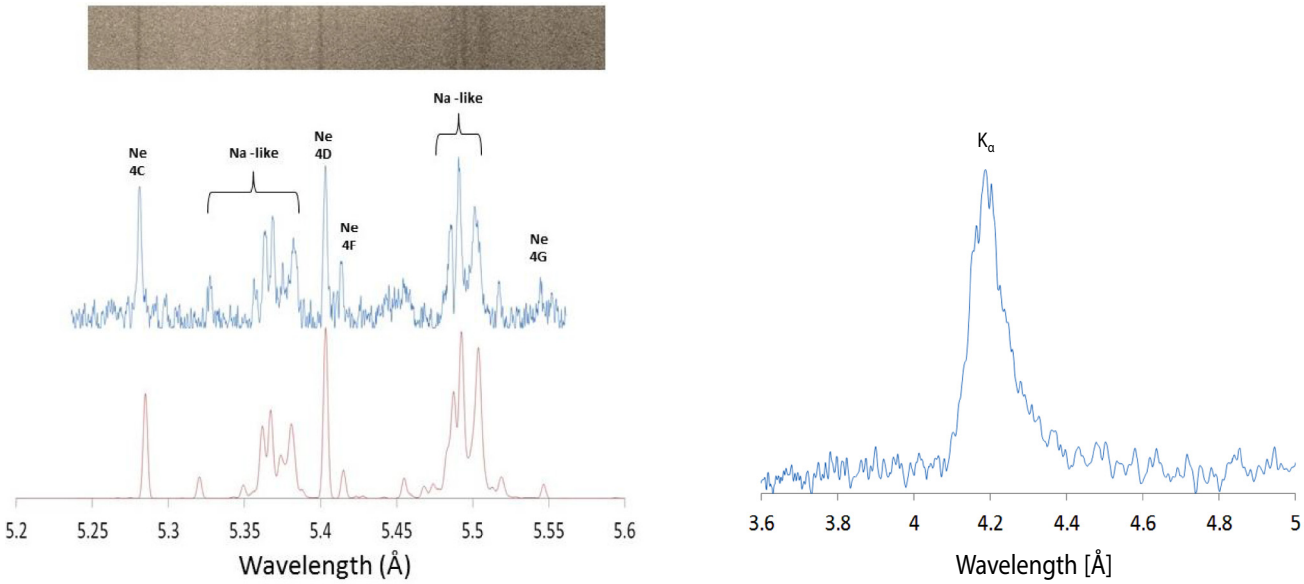

Fig. 15. Kr (left) and Ar (right) x-ray spectra from Ar/Kr mixture supersonic cluster/gas jet produced by short laser pulse (top left blue line). A Johann type spectrometer with Si crystal is used. Laser energy – 14.5 J. Laser flux density 2×10^{19} W/cm^2 in 10 μm size focusing spot. Distance between laser beam axis and nozzle output was 1 mm. Theoretical synthetic spectra (bottom left red line) calculated at Te = 450 eV and $n_e = 10^{21}$ cm^{-3}.

intensity in focus spot of 10^{16} and 2×10^{19} W/cm^2, respectively, was studied. X-ray emission from gas jets generated by a supersonic linear nozzle and cylindrical tube subsonic nozzle was compared. Diagnostics include fast filtered x-ray detectors, x-ray spectrometers, x-ray pinhole cameras, and electron beam Faraday cup detectors. Non-LTE modeling of observed K-shell Ar and L-shell Kr spectra, that displayed the spectra features specific to the certain ionization stages, provided estimates of the electron temperatures and densities and also indication of whether the electron beams were present through observation of lower ionization stages and the "cold" Kα line of Ar (for pure Ar and Ar/Kr mixture experiments).

One of the most intriguing results was that the largest x-ray yield was from the Kr/Ar mixture jet with relatively low Kr concentration. The initial idea about higher x-ray generation efficiency of Kr/Ar mixture irradiated by a short laser pulse was based on the premise that cluster formation at the laser focus spot may be enhanced by adding an impurity gas (Kr in these experiments, and Xe in future) with lower ionization potential of outer electronic shell to the main carrier gas (Ar). By adding to carrier gas Ar easily ionizable seed Kr heavy atoms, ionization processes will begin from high initial ionization stage that will lead to faster ionization and finally to increasing of x-ray yield from plasma. Also, adding of Kr to Ar provided us capability to expand generated x-ray spectra in harder photons energies compared with pure Ar. Indeed, we obtained experimental confirmation that utilization of a mixture of gases instead of single gas is promising. X-ray radiation in a wide spectral region (1–9 keV) from Kr/Ar mixture was 1.5–2 times larger than that from Ar and 20% larger than from Kr. Also, from spectroscopic

Table 1
Average total energy emitted in 4π solid angle and average ε (coefficient of conversion of laser energy to x-ray) in spectral region >2.4 keV measured with absolutely calibrated PCD detectors (delay time 1000 μs, backing pressure 600 psi) at laser intensity 2×10^{19} W/cm^2. The short laser pulse.

Average total energy in 4π above 2.4 keV	Horizontal PCD (mJ) 15° diag. group/ε	Vertical PCD (mJ) vert. diag. group/ε
Ar	7.2	1.3
	4.7×10^{-4}	8.4×10^{-5}
Kr	8.8	3.3
	5.6×10^{-4}	2.1×10^{-4}
15% Kr–85% Ar	10.8	2.3
	7.2×10^{-4}	1.5×10^{-4}

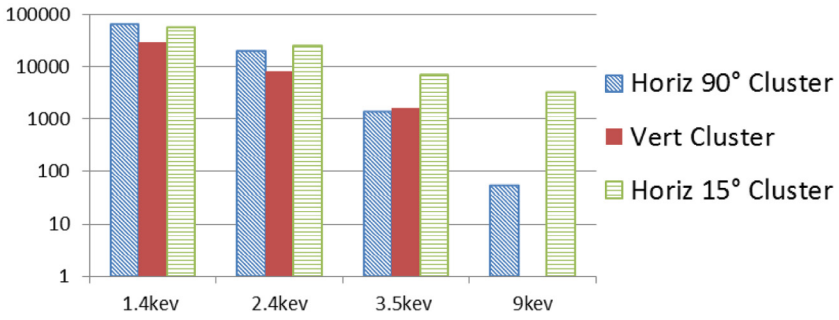

Fig. 16. Normalized spectral integrated distribution of x-ray emission (that include line, recombination, and Bremsstrahlung radiation) from 15%Kr/85%Ar jet in wide spectral range at laser beam intensity 10^{19} W/cm^2. Vertical axis shows x-ray intensity in arbitrary units, horizontal axis shows x-ray photon energy in selected energy bins. Term "cluster" in this illustration means a group of x-ray detectors. Shot # 1594. Delay time 1000 μs, backing pressure 600 psi. The short laser pulse.

measurements it was observed that Ar might not form clusters in the Kr/Ar jet.

The estimation of the maximum conversion coefficient of laser energy to x-rays in the 1.4–3.5 keV spectral region indicated that for the Kr/Ar mixture it is on the order of $\varepsilon \sim 10^{-4}$–10^{-3}. It was observed that for laser pulses with the same energy and comparable jet parameters the short laser pulse generates much higher x-ray burst than the long pulse. The energy yield in the 1–3 keV region produced by supersonic jets irradiated by the short laser pulse was an order of magnitude higher than that produced from subsonic jet. The observed differences are attributed to the presence of clusters in the supersonic jet.

Another intriguing result was that the x-ray radiation from Ar, Kr, as well as 15%Kr/85%Ar jet is emitted anisotropically, with maximum emission radiated perpendicular to the laser beam polarization. The observed anisotropy could be explained by excitation of electron oscillations in the direction of the laser electric field. This would give rise to dipole radiation that is strongest orthogonal to the laser beam polarization direction [29,30], and should be amplified by the presence of dense clusters in the supersonic jets with initial density inside clusters around 10^{23} cm^{-3}. The source x-ray yield can be controlled by changing the gas delay time and the initial density of jet in focus spot. It is an advantage unique to gas-puff jet targets.

In summary, it was found that highly non-uniform plasmas generated during the interaction of short laser pulses with Ar, Kr, and especially Kr/Ar mixture supersonic jets are debris-free strong sources of x-rays in wider spectral region (0.7–9 keV) with a compact bright core. The observed shape of the x-ray pulses from supersonic jets, with sharp forefront and gently sloping trailing edge, was explained with molecular dynamic code and taking into account the presence of a laser post-pulse. A potential evidence of electron beam generation in supersonic jets' plasma was found from x-ray spectroscopic data and a Faraday cup detector data.

Note that the described debris-free gas-puff jet x-ray source can generate x-ray pulses in the repetition regime (at least up to 100–1000 Hz) with application of high repetition short pulse lasers. This is a great advantage as opposed to sources with solid laser targets. The results of recent experiments with Xe/Kr/Ar mixture jets and pure Xe jets will be described in future papers.

Acknowledgements

The authors would like to thank A.A. Esaulov for the theoretical modeling of linear supersonic nozzle. This work was supported by the Defense Threat Reduction Agency, Basic Research Award #HDTRA1-13-1-0033, to the University of Nevada, Reno, and in part by the NNSA under DOE Cooperative Agreements DE-NA0001984 and DE-NA0002075.

References

[1] E.I. Moses, Fusion Sci. Technol. 44 (2003).
[2] S. Bagchi, P. Prem Kiran, K. Yang, A.M. Rao, M.K. Bhuyan, M. Krishnamurthy, et al., Phys. Plasmas 18 (2011) 014502.
[3] K.Y. Kim, H.M. Milchberg, A.Y. Faenov, A.I. Magunov, T.A. Pikuz, I.Y. Skobelev, Phys. Rev. E 73 (2006) 066403.
[4] F. Hagena, Rev. Sci. Instrum. 63 (1992) 2374.
[5] T. Ditmire, T. Donnelly, A.M. Rubenchik, R.W. Falcone, M.D. Perry, Phys. Rev. A 53 (1996) 3379.
[6] I. Alexeev, T.M. Antonsen, K.Y. Kim, H.M. Milchberg, Phys. Rev. Lett. 90 (2003) 103402.
[7] T. Caillaud, F. Blasco, C. Bonté, F. Dorchies, P. Mora, Phys. Plasmas 13 (2005) 033105.
[8] J. Zweiback, T. Ditmire, M.D. Perry, Phys. Rev. A 59 (1999) R3166.
[9] U. Saalmann, C. Siedschlag, J.M. Rost, J. Phys. B At. Mol. Opt. Phys. 39 (2006) R39.
[10] L.M. Chen, F. Liu, W.M. Wang, M. Kando, J.Y. Mao, L. Zhang, et al., Phys. Rev. Lett. 104 (2010) 215004.
[11] L. Zhang, L.M. Chen, D.W. Yuan, W.C. Yan, Z.H. Wang, C. Liu, et al., Opt. Express 19 (2011) 25812.
[12] N.L. Kugland, P. Neumayer, T. Döppner, H.-K. Chung, C.G. Constantin, F. Girard, et al., Rev. Sci. Instrum. 79 (2008) 10E917.
[13] H. Fiedorowicz, A. Bartnik, M. Szczurek, E.E. Fill, Y. Li, P. Lu, et al., Proc. SPIE Int. Soc. Opt. Eng. 2520 (1995) 55.
[14] P.W. Wachulak, A. Bartnik, H. Fiedorowicz, R. Jarocki, J. Kostecki, M. Szczurek, Nucl. Instrum. Methods Phys. Res. B 276 (2012) 38.
[15] P.W. Wachulak, Ł. Węgrzyński, Z. Zápražný, A. Bartnik, T. Fok, R. Jarocki, et al., Appl. Phys. B 117 (2014) 253.
[16] O. Abraham, S.S. Kim, G.D. Stein, J. Chem. Phys. 75 (1981) 402.
[17] V.L. Kantsyrev, A.S. Safronova, I. Shrestha, J.J. Moschella, V.V. Shlyaptseva, K.A. Schultz, et al., 2014 IEEE 41st International Conference on Plasma Sciences (ICOPS) held with 2014 IEEE International Conference on High-Power Particle Beams (BEAMS), 2014, doi:10.1109/PLASMA.2014.7012502.
[18] W.W. Macy, Appl. Opt. 22 (1983) 3898.
[19] F. Dorchies, F. Blasco, T. Caillaud, J. Stevefelt, C. Stenz, A.S. Boldarev, et al., Phys. Rev. A 68 (2003) 023201.
[20] A.S. Safronova, V.L. Kantsyrev, A.Y. Faenov, U.I. Safronova, P. Wiewior, N. Renard-Le Galloudec, et al., High Energy Density Phys. 8 (2012) 190.
[21] E. Biémont, P. Quinet, A.Y. Faenov, I. Skobelev, J. Nilsen, V.M. Romanova, et al., Phys. Scripta 61 (2000) 555.
[22] J. Abdallah Jr., A.Y. Faenov, I.Y. Skobelev, A.I. Magunov, T.A. Pikuz, T. Auguste, et al., Phys. Rev. A 63 (2001) 032706.
[23] M.F. Gu, Can. J. Phys. 86 (2008) 675.
[24] S.B. Hansen, A.S. Shlyaptseva, Phys. Rev. E 70 (2004) 036402.
[25] J. Abdallah Jr., G. Csanak, Y. Fukuda, Y. Akahane, M. Aoyama, N. Inoue, et al., Phys. Rev. A 68 (2003) 063201.
[26] S.B. Hansen, A.S. Shlyaptseva, A.Y. Faenov, I.Y. Skobelev, A.I. Magunov, T.A. Pikuz, et al., Phys. Rev. E 66 (2002) 046412.
[27] G.M. Petrov, J. Davis, A.L. Velikovich, P.C. Kepple, A. Dasgupta, R.W. Clark, et al., Phys. Rev. E 71 (2005) 036411.
[28] G.M. Petrov, J. Davis, A.L. Velikovich, P. Kepple, A. Dasgupta, R.W. Clark, Phys. Plasmas 12 (2005) 063103.
[29] O.N. Krokhin, Y.A. Mikhailov, V.V. Pustovalov, A.A. Rupasov, V.P. Silin, G.V. Sklizkov, et al., JETP Lett. 20 (1974) 105.
[30] S. Kranzusch, C. Peth, K. Mann, Rev. Sci. Instrum. 74 (2003) 969.